Available online at www.sciencedirect.com

SciVerse ScienceDirect

Acta Materialia 60 (2012) 487–497

Acta MATERIALIA

www.elsevier.com/locate/actamat

Effect of second phase particles on grain refinement during equal-channel angular pressing of an Al–Mg–Mn alloy

I. Nikulin *, A. Kipelova, S. Malopheyev, R. Kaibyshev

Laboratory of Mechanical Properties of Nanoscale Materials and Superalloys, Belgorod State University, Pobeda 85, Belgorod 308015, Russia

Received 7 June 2011; received in revised form 12 October 2011; accepted 13 October 2011
Available online 22 November 2011

Abstract

The process of grain refinement under severe plastic deformation was examined in an Al–5.4% Mg–0.5% Mn–0.1% Zr alloy, which was subjected to equal-channel angular pressing (ECAP) in the strain interval from 1 to 12 at a temperature of ~300 °C. It was shown that the size and distribution of the second phase particles precipitated under homogenization annealing strongly affect grain refinement. Extensive grain refinement under ECAP was provided by a dispersion of Al_6Mn particles with an average size of ~25 nm that precipitated during the homogenization annealing at an intermediate temperature. The fully recrystallized structure with an average crystallite size of ~0.55 μm evolves through continuous dynamic recrystallization. In contrast, homogenization annealing at a high temperature leads to the formation of coarse Al_6Mn particles with a plate-like shape. Under further ECAP, the formation of coarse recrystallized grains takes place in this material due to the discontinuous growth of recrystallized grains during the inter-pass annealing between the ECAP passes. The role of second phases in grain refinement is discussed in terms of pinning and driving forces for recrystallization.

Keywords: Aluminum alloys; Precipitation; Severe plastic deformation; Dynamic recrystallization; Ultra-fine-grained structure

1. Introduction

Non-age-hardenable Al–Mg alloys with moderate strength are widely used because of their excellent corrosion resistance, formability and weldability [1]. The main strengthening effects of these alloys come from solid solution strengthening and strain hardening [1]. It has been shown that the strength of Al–Mg alloys can be increased by extensive grain refinement using equal-channel angular pressing (ECAP) [2–4]. For example, Hayes et al. [3] reported that the yield strength of the Al–3% Mg alloy with a submicron structure produced by ECAP is comparable to that obtained by age-hardening in wrought Al–Cu alloys. It is known [5,6] that in severe plastic deformation (SPD) processing, a steady-state grain size is eventually reached at ultra-high strains that limits the achievable level of grain refinement. This limit is controlled by the mobility of low- and high-angle grain boundaries. The introduction of second-phase particles, which effectively pin grain boundaries, is a method for decreasing the limiting grain size [7], allowing an increase in strength. Alloying elements such as Zr and Sc, which form nanoscale dispersoids that exert Zener drag pressure [8], are often added to Al–Mg alloys for this purpose. Scandium, which forms coherent Al_3Sc dispersoids with sizes ranging from 5 to 25 nm [9], effectively retards the onset of static recrystallization up to pre-melting temperatures [10,11]. However, the high cost of Sc restricts the commercial application of Sc-containing Al–Mg alloys to a limited range of low-volume, high-performance components, primarily for use in the aerospace industry, and prevents the expansion of these alloys into the fabrication of high-volume components associated with the automotive and shipbuilding industries. To overcome these economic limitations, an important current objective is the development of the chemistry of Al–Mg alloys and processing routes that are capable of the easy production of ultra-fine-grained (UFG) microstructures by ECAP

* Corresponding author. Tel.: +7 4722 585457; fax: +7 4722 585417.
E-mail address: nikulin.i.a@gmail.com (I. Nikulin).

1359-6454/$36.00
doi:10.1016/j.actamat.2011.10.023

and, as a result, achieving high strength in commercial Al–Mg alloys without Sc.

Several studies have focused on the examination of the grain refinement processes in Al–Mg alloys with and without dispersed second phase particles under ECAP [2,7,12,13]. There is some confusion in the literature about the effect of nanoscale dispersoids on the formation of UFG structures under SPD. Apps et al. [7,12] compared the grain refinement processes in a binary Al–0.2% Sc and a single-phase Al–0.13% Mg alloy and showed that the presence of coherent Al_3Sc dispersoids retards the formation of a UFG structure because they reduce the rate of high-angle grain-boundary development at moderate strains. On the contrary, Ning et al. [13] examined the effect of Zr on the grain refinement process during ECAP of an Al–4.6% Mg–0.6% Mn alloy and showed that the formation of incoherent Al_3Zr dispersoids provides some decrease in final grain size and inhibits the recrystallization processes in the UFG structure under static annealing. However, there is no detailed information on the effect of Al_3Zr dispersoids on the grain refinement process during ECAP. Barlow et al. [14] reported that the introduction of nanoscale dispersoids into an aluminum matrix accelerates the grain refinement because of enhanced dislocation generation and the reduction of the slip distances. On the over hand, it has also been noted [7,12] that the presence of dispersoids has been found to homogenize slip, retard the formation of a cellular substructure and inhibit the formation of microshear bands during deformation. Thus, the effect of the dispersed phase particles on the UFG structure formation has not been clearly determined.

In this study, a commercial Al–5.4% Mg–0.5% Mn–0.1% Zr alloy, denoted 1561Al, was used to study the effect of the dispersed particles on the grain refinement processes during SPD. This alloy contains Zr, which can form incoherent nanoscale Al_3Zr dispersoids. However, Zr is peritectic with Al, having a maximum usable solid solubility of ~0.14wt.% [15,16]. As a result, the volume fraction of the Al_3Zr dispersoids is typically small. In addition, in Al–Mg–Mn alloys, coarse particles of the Al_6Mn phase with a plate-like shape typically develop during homogenization annealing at high temperatures [16–18]. It is also possible to produce a dispersion of the nanoscale Al_6Mn phase that exhibits an equiaxed shape by performing the homogenization annealing at an intermediate temperature [19]. Thus, the 1561Al alloy can be produced in two states that are distinguished by the shape and size of their secondary phases, allowing investigation of their effect on the grain refinement. The aim of this study is to examine the dependence of the grain refinement process on the size and distribution of the second-phase particles in a commercial Al–5.4% Mg–0.5% Mn–0.1% Zr alloy.

2. Material and experimental procedure

The commercial 1561Al alloy with a chemical composition of Al–5.4% Mg–0.5% Mn–0.1% Zr–0.12% Si–0.014% Fe (in wt.%) was manufactured by direct chill casting, with a solidification rate of $100\ ^\circ C\ s^{-1}$. The ingots were then subjected to a homogenization annealing (HA) treatment by one of two routes. In the first HA treatment, the ingot was annealed at 360 °C for 6 h. In the second HA treatment, the ingot was annealed at 440 °C for 12 h, followed by final annealing at 500 °C for 12 h. The alloys annealed by one of the two HA treatments were designated 1561HA1 and 1561HA2.

Both ingots were machined into rods with dimension of 20 mm × 20 mm × 100 mm. These rods were subjected to ECAP at a temperature of ~300 °C using an isothermal die with a channel having a square cross-section of 20 mm × 20 mm. The channel had an L-shaped configuration, with an angle of intersection of 90° and an outer arc curvature angle of ~1°. Deformation through this die produced a strain (ε) of ~1 with each passage [20]. All of the billets were processed by ECAE to 1, 2, 4, 8 and 12 passes using route B_c [2]. The pressing speed was $\sim 3\ mm\ s^{-1}$. Finally, the extruded rods were water quenched. The specimens were exposed within an isothermal die at 300 °C for 2 min before each pass.

The specimens for microstructural examination were cut from the central area of the extruded rods, parallel to the extrusion direction. For the electron-backscattering diffraction (EBSD) analysis, these specimens were slightly electropolished at −30 °C in a solution of 30% HNO_3 and 70% CH_3OH to produce a strain-free surface. The EBSD orientation maps were recorded using a FEI Quanta 600FEG scanning electron microscope fitted with a high-resolution EBSD analyzer. The arbitrary area was automatically scanned with a step size of ~0.1 μm. No boundaries with misorientation less than 2° were taken into account. In the data presented, high-angle boundaries (HABs) were defined by a misorientation of $\theta \geqslant 15^\circ$, and low-angle boundaries (LABs) were defined by $2^\circ < \theta < 15^\circ$. HABs and LABs are depicted in the EBSD maps as black and white lines, respectively. The terms "grains" and "subgrains" are used for the definition of crystallites, which are entirely delimited by HABs and LABs, respectively. The term "(sub)grains" refers to crystallites that are bounded partly by LABs and partly by HABs. The volume fraction of ultra-fine grains was deemed to be the "recrystallized" fraction. The "crystallite size" is defined as the mean separation of all boundaries (HABs and LABs). The foils were examined using a JEM-2100 transmission electron microscope (TEM) operating at 200 kV and fitted with an INCA energy-dispersive X-ray spectrometer (EDXS). The second phase particles were identified by both EDXS analysis and selected area diffraction. The volume fraction of the second phase particles, f, was measured in accordance with Ref. [21]. The dislocation density was estimated by counting individual dislocations crossing the thin foil surface [22]. The misorientations on the (sub)grain boundaries were studied using a conventional Kikuchi-line technique in TEM [23].

3. Experimental results

3.1. Microstructure after homogenization annealing

A granular structure with an average grain size of ~250 μm was observed in both states of the 1561Al alloy (Fig. 1a and b). Nanoscale incoherent dispersoids identified as Al_6Mn phase with an average diameter of ~25 nm were observed in the 1561Al alloy after HA1 treatment (Fig. 1c). The volume fraction of these dispersoids was ~0.025. In contrast, the 1561HA2 alloy contains coarse, plate-like Al_6Mn particles with average dimensions of ~150 nm by 60 nm in the longitudinal and transversal direction, respectively (Fig. 1d). The volume fraction of the coarse plate-like particles was ~0.02.

In addition, primary Mg_2Si and Mg_2Al_3 particles with an average size of ~200 nm and Mg_2Si particles with an average size of ~90 nm were observed after homogenization in the 1561HA1 and 1561HA2 alloys, respectively. In both alloys, the volume fraction of these particles was significantly lower than 0.001. As a result, these particles have no impact on the grain refinement processes.

The 1561Al alloy was carefully examined by TEM in an attempt to observe the formation of Al_3Zr dispersoids during HA. However, no Al_3Zr dispersoids were found after either HA treatment. EDXS analysis has shown that Zr is retained in the supersaturated solid solution after homogenization annealing in the 1561Al alloy processed with the HA1 and HA2 treatments. It has previously been found that annealing in the temperature interval 450–500 °C for at least 200 h is necessary for the precipitation of fine Al_3Zr dispersoids [15,24].

3.2. Deformation microstructure

3.2.1. The 1561HA1 alloy

Typical EBSD maps and the profiles of point-to-point ($\Delta\theta$) and cumulative point-to-origin ($\Sigma\Delta\theta$) misorientations of the deformation microstructure developed during ECAP in the 1561HA1 alloy are shown in Figs. 2 and 3, respectively. It can be seen in Fig. 2a that the microstructures developed at $\varepsilon \approx 1$ are characterized by the elongation of the original grains in shear direction, and the formation of extended LABs is observed within the interiors of the original grains. These LABs comprise deformation bands and are aligned in the shear direction as the original boundaries. The TEM results reveal that the deformation bands delimitated by LABs in the shear direction and containing high dislocation density ($\rho \sim 1.6 \times 10^{14}\,m^{-2}$) are subdivided in the transverse direction by dislocation walls with a misorientation of $\theta < 3°$ (Fig. 4a). The formation of dislocation walls within the deformation bands leads to the formation of highly elongated subgrains and (sub)grains with an average misorientation of deformation-induced boundaries of $\theta av \approx 3.3°$. It can be seen (Fig. 3a) that the point-to-point misorientation attains a value of ~10° near

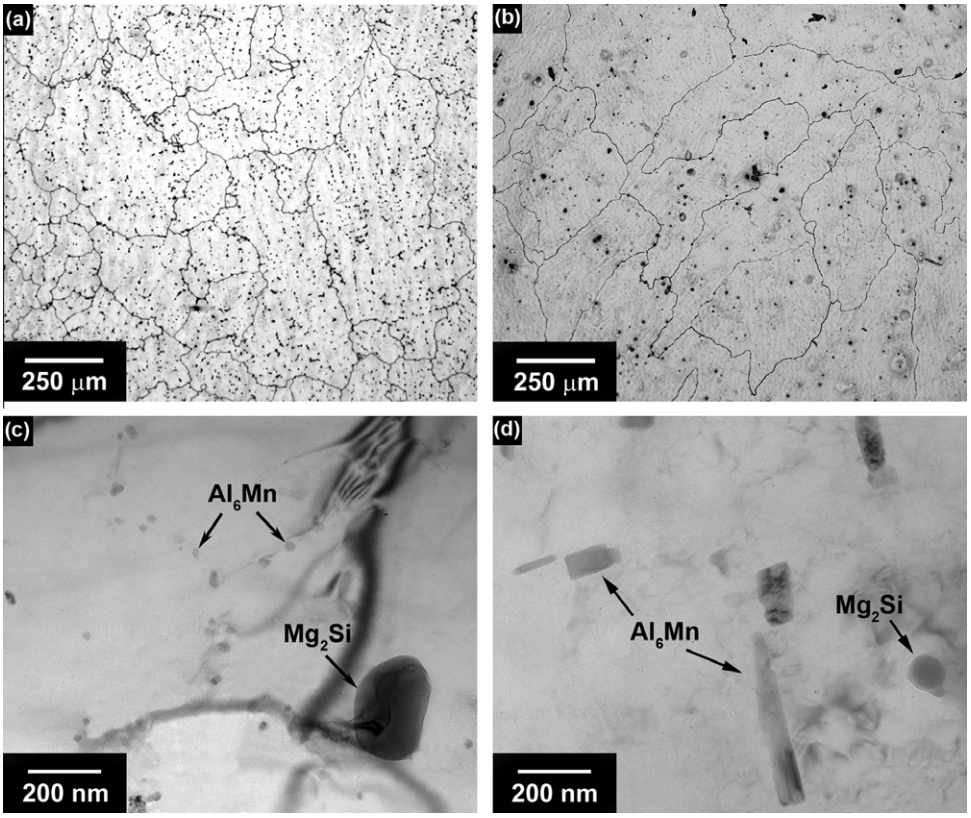

Fig. 1. Microstructure of the 1561HA1 alloy (a,c) and the 1561HA2 alloy (b,d). Optical (a,b) and TEM (c,d) micrographs.

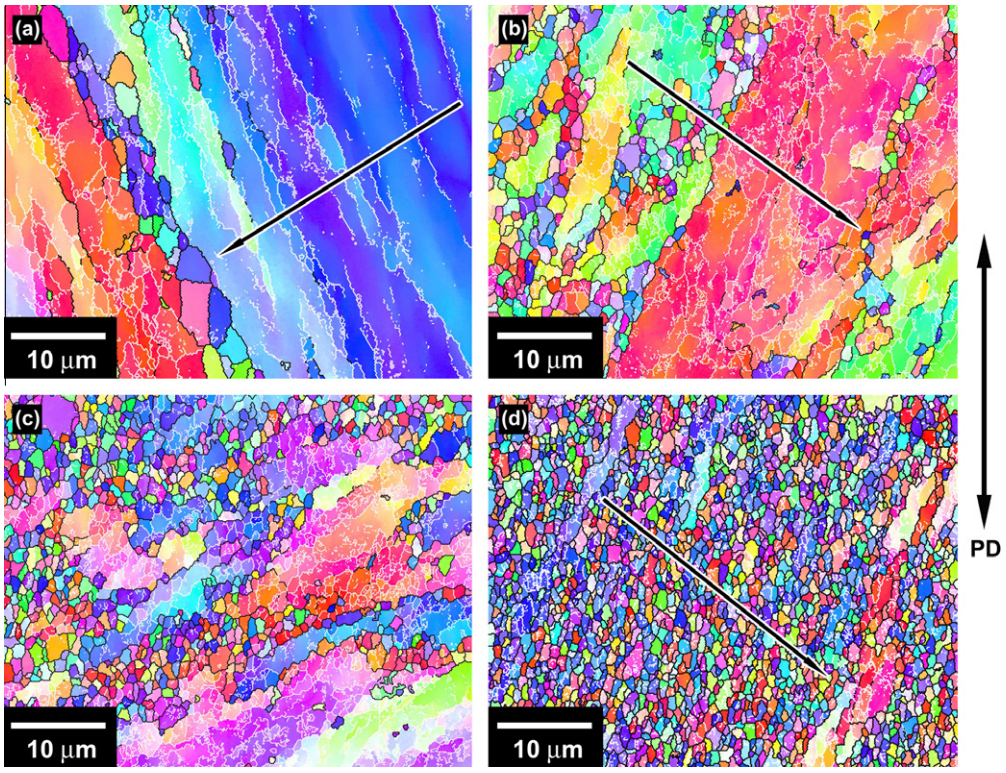

Fig. 2. Typical EBSD maps of the 1561HA1 alloy processed by ECAP at 300 °C to various strains: (a) $\varepsilon \approx 1$, (b) $\varepsilon \approx 4$, (c) $\varepsilon \approx 8$ and (d) $\varepsilon \approx 12$. PD is the pressing direction.

the original grain boundary, while the value of $\Delta\theta$ does not exceed 5° at a distance from the boundary. This difference suggests a higher misorientation at the original grain boundaries than in the core region (Fig. 3a). The continuous change of $\Sigma\Delta\theta$ within the deformation bands is attributed to lattice distortions due to the dislocation tensor, indicative of a deformation gradient in those locations. As a result, chains of recrystallized grains evolve along separate initial boundaries (Fig. 2a).

Deformation to $\varepsilon \approx 4$ leads to the formation of new fine grains surrounded by HABs (Fig. 2b). The TEM observation of the 1561HA1 alloy shows that the original grains mainly consist of deformation bands and subgrains (Fig. 4b) with a dislocation density of $\sim 1.5 \times 10^{14}\ m^{-2}$. It was also observed that the subgrains tend to acquire an equiaxed shape with strain. The moderate dislocation density of $\sim 5 \times 10^{13}\ m^{-2}$ was observed in areas of new recrystallized grains. It is worth noting that the new grains are highly misoriented to each other (Fig. 3b), and most of the deformation-induced (sub)grains and grains exhibit an equiaxed shape (Fig. 2b) that is in contrast with lower strains. The cumulative misorientation changes abruptly in areas of new developed grains, while it changes continuously in subgrain areas, suggesting deformation heterogeneity (Fig. 3b).

With further deformation to higher strains, the number of new grains continuously increases. At $\varepsilon \approx 8$, in addition, the formation of recovered subgrains takes place within interiors of original grains (Fig. 2c). These equiaxed grains and subgrains are characterized by a slightly decreased dislocation density ($\rho \sim 8 \times 10^{13}\ m^{-2}$). At $\varepsilon \approx 12$, the fully recrystallized structure evolves (Figs. 2d and 3c); subgrains are rarely observed. The variation of the cumulative misorientation within a new grain is negligibly small (Fig. 3c); however, crystallites with a moderate dislocation density of $\sim 7.7 \times 10^{13}\ m^{-2}$ are still visible (Fig. 4c). As can be seen in Fig. 2d, the formation of the uniform UFG microstructure is almost completed at $\varepsilon \approx 12$.

3.2.2. The 1561HA2 alloy

The misorientation maps of the 1561HA2 alloy subjected to ECAP are shown in Fig. 5. At a strain of ~1, the original grains are elongated in the shear direction and are subdivided on coarse deformation bands by LABs (Fig. 5a). The microstructure that evolves in the 1561HA2 alloy at $\varepsilon \approx 1$ is similar to that developed in the 1561HA1 alloy after a single ECAP pass (Figs. 2a and 5a). However, in the 1561HA2 alloy, the width of the deformation bands is significantly larger; transverse LABs are rarely observed by EBSD analysis within these bands (Fig. 5a). The TEM results shown in Fig. 7a reveal that the transversal LABs are mainly the dislocation walls, with the dominant misorientation ranging from 0.6° to 2.5°. The local average misorientation of the deformation structures developed at $\varepsilon \approx 1$ is ~2°, which is significantly less than that in the 1561HA1 alloy. The cumulative misorientation changes within tens of degrees in the deformation bands (Fig. 6a), indicating the existence of

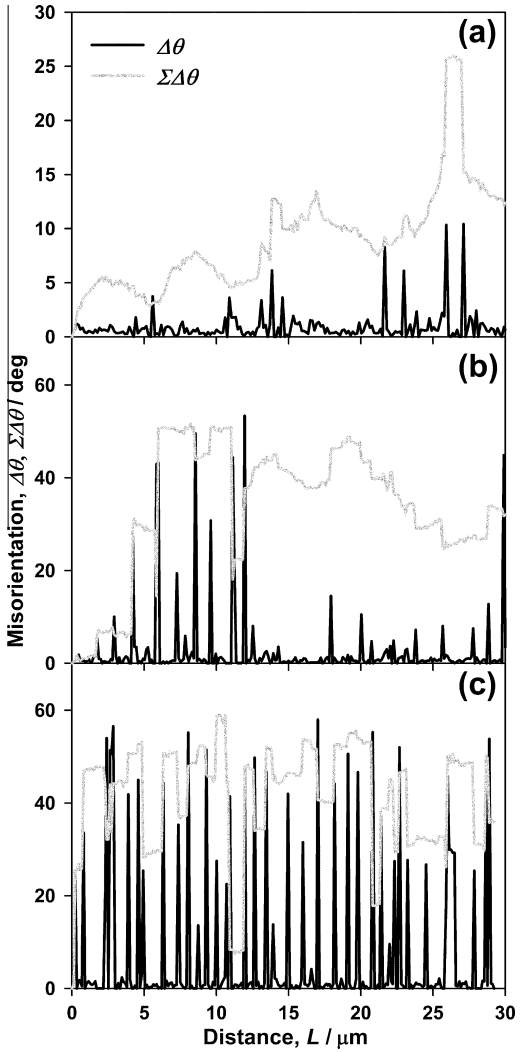

Fig. 3. Point-to-point ($\Delta\theta$) and point-to-origin ($\Sigma\Delta\theta$) misorientation of strain-induced boundaries developed along lines pointed at Fig. 2: (a) $\varepsilon \approx 1$, (b) $\varepsilon \approx 4$, (c) $\varepsilon \approx 12$.

significant deformation gradient within the interiors of the deformation bands. The overall dislocation density of $\sim 4.9 \times 10^{13}\ m^{-2}$ is three times lower than that in the 1561HA1 alloy.

With further deformation to $\varepsilon \approx 2$, the number of recrystallized grains (Fig. 5b) increases and the cumulative misorientation within the interiors of the original grains (Fig. 6b) flattens. Coarse recrystallized grains containing a dislocation density $\rho < 10^{13}\ m^{-2}$ (Fig. 7b) alternate with deformation bands containing a moderate dislocation density of $\sim 4.6 \times 10^{13}\ m^{-2}$. This structure is typical for the local static growth of some crystallites during the exposure between ECAP passes [25]. Static grain growth results in the formation of a bimodal structure consisting of coarse grains and (sub)grains with a slightly elongated shape located in deformation bands.

Further deformation up to $\varepsilon \approx 4$ results in the formation of a microstructure consisting of three types of crystallites (Fig. 5c). The first structural component consists of coarse recrystallized grains (Fig. 5c). These grains are free of lattice dislocations (Fig. 7c). The second structural component is lamellar grains subdivided by LABs into (sub)grains exhibiting an equiaxed shape. The third structural component comprises fine recrystallized grains that exhibit an equiaxed shape (Fig. 5c) and contain a moderate number of lattice dislocations (Fig. 7c). The fraction of fine recrystallized grains is relatively small in the microstructure that develops at $\varepsilon \approx 4$ in the 1561HA2 alloy. The dislocation density was measured to be $\sim 3.9 \times 10^{13}\ m^{-2}$ within the subgrain and grain areas. Upon further straining, the number of fine and coarse recrystallized grains tends to increase (Fig. 5d). However, the coarse grains (i.e., the first structural component) dominate at $\varepsilon \geqslant 4$ (Fig. 5c and d). Note that the dislocation densities of $\sim 3.8 \times 10^{13}\ m^{-2}$ that were measured within the subgrain and grain interiors at $\varepsilon \approx 12$ are almost the same as those in the 1561HA2 alloy deformed to $\varepsilon \approx 4$.

3.3. Dispersoids

TEM observation of the deformation structure of the 1561HA1 alloy showed that the size of Al_6Mn dispersoids decreases slightly during the hot ECAP at $\varepsilon > 4$ (Fig. 4c). The mean diameter of the particles is ~22 nm. The volume fraction of the Al_6Mn particles is ~0.025, which is the same as in the as-homogenized 1561HA1 alloy. These particles can effectively pin mobile dislocations (Fig. 4c) and, because of increased Zener drag pressure, hinder the mobility of the grain boundaries [8].

An examination of the deformed structure of the 1561HA2 alloy showed that coarse Al_6Mn particles that precipitate during the high-temperature homogenization annealing remain in the structure up to high values of the strain. Moreover, a small number of additional fine Al_6Mn dispersoids with an average diameter of ~22 nm precipitate in the 1561HA2 alloy at $\varepsilon \geqslant 8$ (Fig. 7d). These newly formed dispersoids are predominantly located within areas of fine grains, while the coarse Al_6Mn particles are randomly distributed throughout the alloy body. It seems that in the 1561HA2 alloy, the fine recrystallized grains can retain their dimensions in areas where the additional precipitation of equiaxed nanoscale Al_6Mn particles takes place. Noticeable grain coarsening occurs under static conditions in the areas in which the coarse plate-like Al_6Mn particles are the dominant phase.

Thus, the fine Al_6Mn particles precipitated under homogenization annealing at intermediate temperature strongly promote extensive grain refinement in the 1561Al alloy. On the other hand, inhomogeneous structure was found to evolve in the 1561HA2 alloy because of the coarse Al_6Mn particles precipitated at high-temperature homogenization. It is obvious that the structural characteristics of finely dispersed Al_6Mn phase particles are critically important for the size of the final recrystallized grains, the uniformity of the recrystallized structure and the rate of the grain refinement process as well.

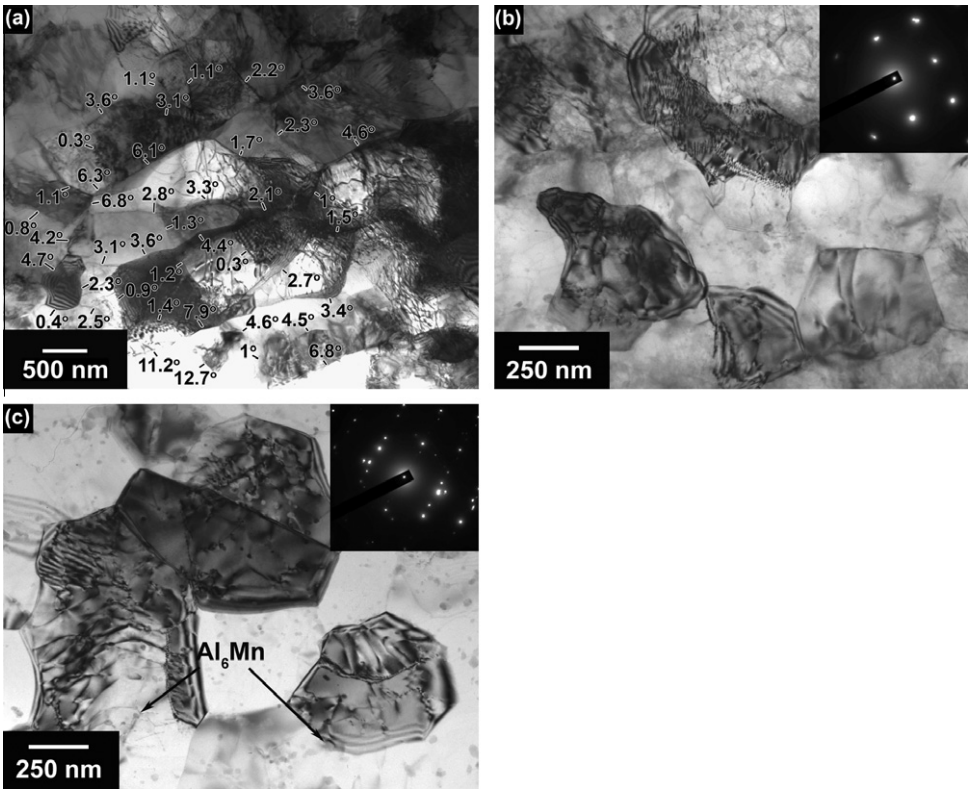

Fig. 4. TEM micrographs of the 1561HA1 alloy deformed to: $\varepsilon \approx 1$ (a), $\varepsilon \approx 4$ (b) and $\varepsilon \approx 12$ (c).

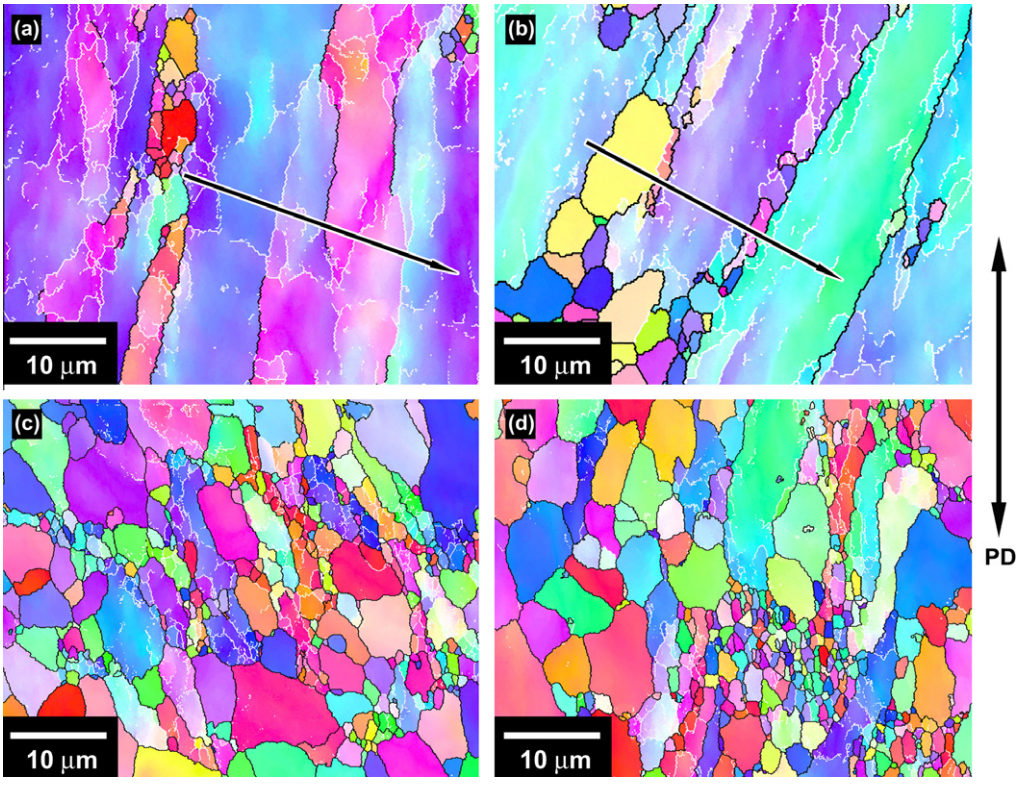

Fig. 5. Typical EBSD maps of the 1561HA2 alloy deformed to: $\varepsilon \approx 1$ (a), $\varepsilon \approx 2$ (b), $\varepsilon \approx 4$ (c) and $\varepsilon \approx 12$ (d). PD is the pressing direction.

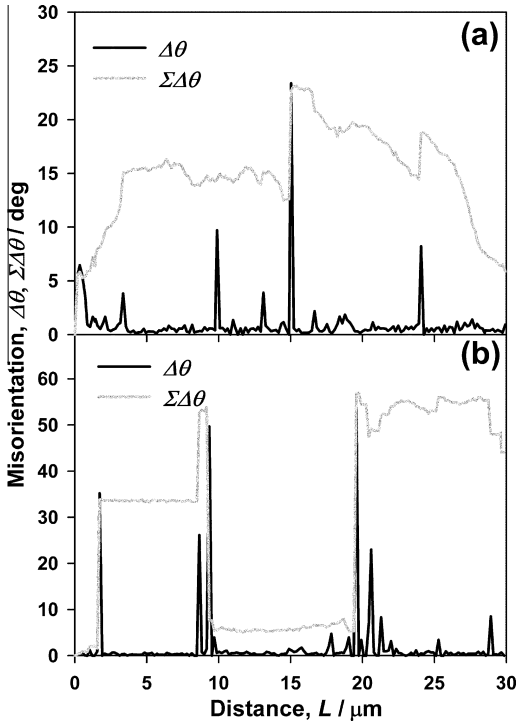

Fig. 6. Point-to-point ($\Delta\theta$) and point-to-origin ($\Sigma\Delta\theta$) misorientation of strain-induced boundaries developed along lines pointed at Fig. 5 (a) and (b): (a) $\varepsilon \approx 1$, (b) $\varepsilon \approx 2$.

3.4. Parameters of microstructure as a function of strain

The effect of strain on the fraction of boundaries is shown in Fig. 8a and b for the 1561HA1 and 1561HA2 alloys, respectively. The HABs are subdivided on medium angle boundaries (MABs) ($15 \leqslant \theta < 30°$) and very high angle boundaries (VHABs) ($30 \leqslant \theta < 62.8°$). In the 1561HA1 alloy, the fraction of LABs continuously decreases from 0.77 to 0.34 as the overall strain increases from 1 to 12. In the 1561HA2 alloy, the fraction of LABs decreases from 0.77 to 0.36 in the strain interval from 1 to 4, and remains virtually unchanged with further straining (Fig. 8b). The increase of strain to $\varepsilon \approx 12$ insignificantly affects the fraction of MABs, which is almost unchanged during deformation for both states of the 1561Al alloy. In the 1561HA1 alloy the fraction of VHABs continuously increases with increasing cumulative strain; at $\varepsilon \approx 12$, the sum of MABs and VHABs is ~0.66. On the other hand, in the 1561HA2 alloy, the fraction of VHABs increases to 0.5 at $\varepsilon \approx 4$ and then remains unchanged in the strain interval from 4 to 12.

The strain dependence of the average misorientation is similar to that of the fraction of VHABs (Fig. 8c). It can be seen that in the 1561HA1 alloy, θav increases continuously from 12 to 28.5° as the strain increases from 1 to 12. In the 1561HA2 alloy, the average misorientation increases rapidly from 11° to 28° in the strain interval from 1 to 4 and remains almost unchanged upon further straining to $\varepsilon \approx 12$. It is worth noting that the continuous increase of the average misorientation in the present alloy takes place because of the incremental growth of the VHABs' portion with strain.

The effect of strain on the average crystallite size measured in the longitudinal direction (i.e. in the direction of grain elongation) and in the transverse direction is summarized in Fig. 8d. It is seen that the size of crystallites tends to decrease gradually with increasing strain in the 1561HA1 and 1561HA2 alloys. In the strain interval from 1 to 4, the crystallite size in the 1561HA1 alloy rapidly decreases because of an increasing fraction of equiaxed crystallites. It is worth noting that the transverse size of the crystallites remains almost unchanged after $\varepsilon \approx 4$, and the longitudinal size of the elongated subgrains approaches the transverse size. It can be clearly seen in Fig. 8d that the temperature of homogenization annealing strongly affects the size of the crystallites developed in the 1561Al alloy during ECAP. For example, at $\varepsilon \approx 12$, the average sizes of the fine crystallites were ~0.55 and 0.7 μm in the 1561HA1 and 1561HA2 alloys, respectively. The decreased crystallite size observed in the 1561HA1 alloy at $4 \leqslant \varepsilon \leqslant 12$ is associated with fine Al_6Mn particles, which promote grain refinement. In the 1561HA2 alloy, which does not contain nanoscale particles, coarse grains start to develop at $\varepsilon \approx 2$. The average size of the coarse grains increases from 4.7 to 5.6 μm with increasing strain.

4. Discussion

The results described above show that the process of grain refinement in the 1561Al alloy under ECAP is strongly dependent on the size and morphology of the Al_6Mn particles precipitated under homogenization annealing. It can be concluded from the present study that the microstructure developed in the 1561Al alloy after ECAP is the result of the superposition of the processes of hot deformation and static recrystallization during annealing. The UFG structure was achieved by an effective strain of ~12 in the alloy containing incoherent Al_6Mn dispersoids, in contrast with the Al–6% Mg alloy containing coherent Al_3Sc particles [25]. The regularities of the grain refinement under ECAP in the 1561HA1 alloy are similar to those in the Sc-bearing Al–Mg alloys [26,27]. It is obvious that the high density of nanoscale Al_6Mn particles with incoherent boundaries facilitates grain refinement in the 1561HA1 alloy. These particles showed high resistance to coarsening at 300 °C under annealing and ECAP conditions as well. Therefore, they may exert high a Zener drag force [8], providing stability of deformation structure under static and dynamic conditions. In contrast, the heterogeneous structure with coarse grains associated with a lack of Zener drag force is developed during ECAP in the 1561HA2 alloy with plate-like Al_6Mn particles.

The ability of the grain boundaries to migrate may be approximately determined from the balance of the driving force for recrystallization (F_d) and the Zener drag force (F_p) caused by small particles. When $F_d \geqslant F_p$, normal grain growth caused by static recrystallization will take place.

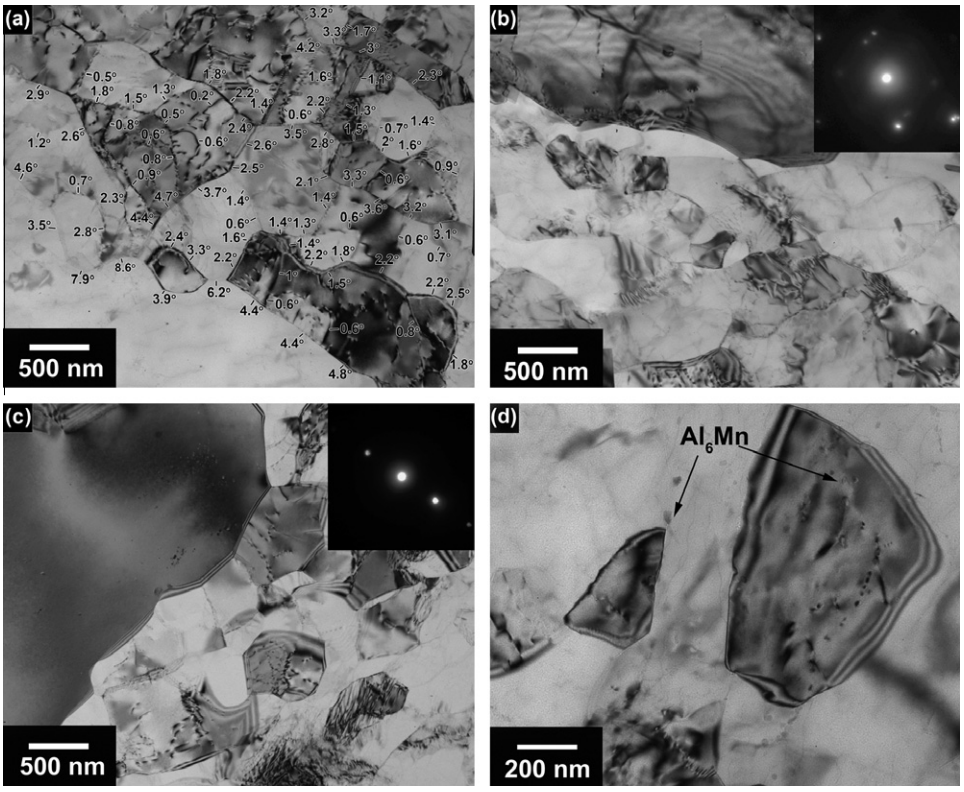

Fig. 7. TEM micrographs of the 1561HA2 alloy deformed to $\varepsilon \approx 1$ (a), $\varepsilon \approx 2$, (c) $\varepsilon \approx 4$ and (d) $\varepsilon \approx 8$.

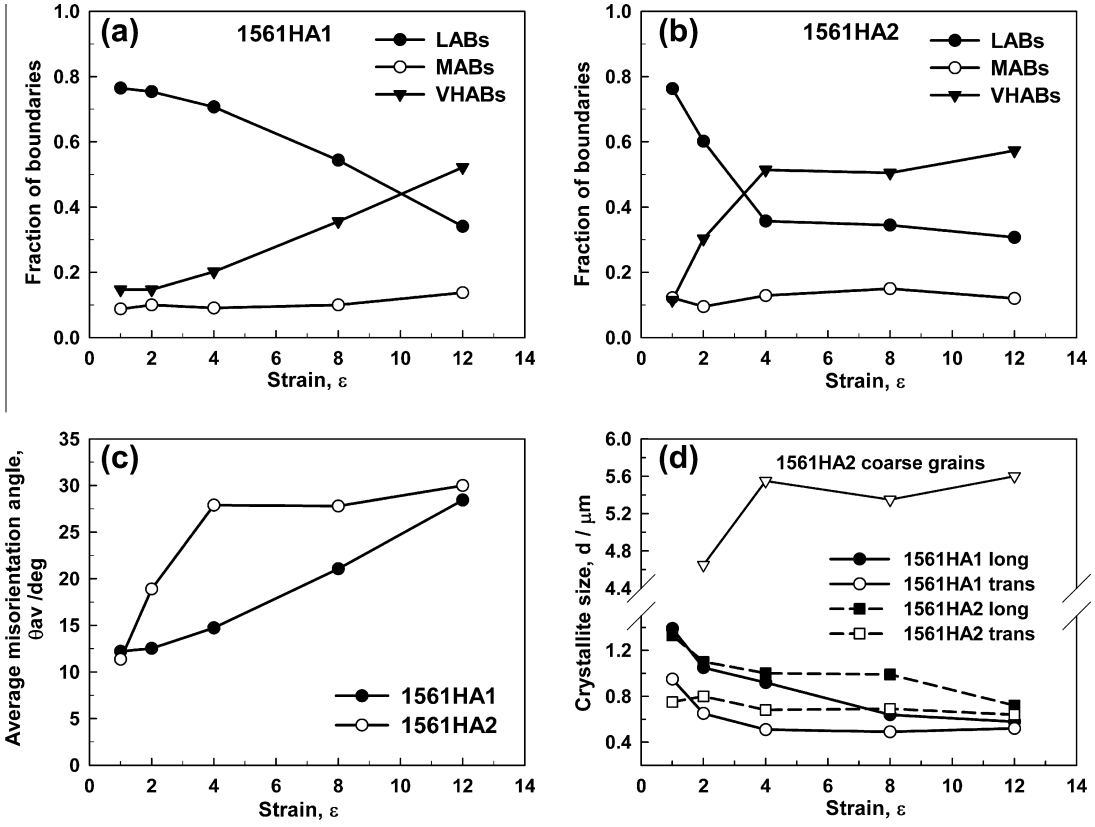

Fig. 8. Effect of strain on (a,b) population of LABs, MABs and VHABs; (c) average misorientation of deformation-induced boundaries, θav; (d) the crystallite size, d (for 1561HA2 alloy, the average size of coarse grains is represented).

The driving force for recrystallization is provided by the accumulated dislocation density, which gives rise to a stored energy [8], given by:

$$F_d = 0.5Gb^2\Delta\rho \quad (1)$$

where $b = 2.86 \times 10^{-10}$ m [8] is the Burgers vector; $G = 1.96 \times 10^{10}$ N m^{-2} [28] is the shear modulus of the Al–Mg–Mn alloy at 300 °C and $\Delta\rho$ is the dislocation density. Substituting the b and G values into Eq. (1) leads to an F_d value in the 1561HA1 alloy of $\sim 1.3 \times 10^5$ N m^{-2} and $\sim 6.2 \times 10^4$ N m^{-2} for the dislocation densities $\Delta\rho \approx 10^{14}$ m^{-2} $(1 \leqslant \varepsilon \leqslant 4)$ and $\Delta\rho \approx 10^{13}$ m^{-2} $(8 \leqslant \varepsilon \leqslant 12)$, respectively.

In the case of randomly distributed spherical incoherent particles, the drag force inhibiting normal grain growth is given by [8]:

$$F_p = 3f\gamma/2r \quad (2)$$

where $f = 0.025$ is the volume fraction of Al_6Mn dispersoids in the 1561HA1 alloy (see Sections 3.1 and 3.3); $\gamma = 0.32$ J m^{-2} [29] is the grain boundary energy of aluminum; and r of ~12.5 and 11 nm is the mean radius of the spherical Al_6Mn dispersoids for the 1561HA1 alloy in the initial and deformed conditions, respectively. The substitution of these values into Eq. (2) gives F_p of $\sim 6.9 \times 10^5$ N m^{-2} and $\sim 9.2 \times 10^5$ N m^{-2} for nanoscale dispersoids of the Al_6Mn phase precipitated under homogenization and deformation at $\varepsilon \geqslant 8$, respectively. These values are, respectively, nearly equal to and higher by a factor of ~1.5 than the value for the Zener drag pressure originating from coherent Al_3Sc dispersoids in the 1570Al alloy [25].

In order to evaluate the drag force originating from the coarse Al_6Mn particles, the following values were used: $f \approx 0.02$ is the volume fraction of Al_6Mn particles in the 1561HA2 alloy; $r \approx 100$ nm, evaluated in accordance with Ref. [8], is the radius of the spherical particles equivalent to the plate-like Al_6Mn particles in the homogenized 1561HA2 alloy. Substitution of these values into Eq. (2) leads to an F_p value of $\sim 1.9 \times 10^5$ N m^{-2}. A driving force of $\sim 3.5 \times 10^4$ N m^{-2} was obtained for the recrystallization of the 1561HA2 alloy with dislocation density $\Delta\rho \approx 4 \times 10^{13}$ m^{-2} $(1 \leqslant \varepsilon \leqslant 12)$.

The ratio $F_p > F_d$ suggests that normal grain growth is completely inhibited on annealing in both states of the 1561Al alloy. However, a coarse grained structure was observed in the 1561HA2 alloy after ECAP. There are two critical levels of pinning, depending on the dispersion of particles [30,31]; at a high pinning force, neither normal nor abnormal grain growth is possible, whereas at a low pinning force, the deformed structure cannot undergo normal grain growth, but abnormal grain growth is still possible. The F_p of Al_6Mn particles in the 1561HA2 alloy is ~5 times that in the 1561HA1, and in the 1561HA2 at $\varepsilon \geqslant 4$, the deformation microstructure discontinuously evolves into coarse and high aspect-ratio recrystallized grains mixed with fine grains (i.e., a bimodal structure is formed) (Figs. 5 and 7).

The theory [32] predicts the ability of the 1561Al alloy to undergo grain coarsening during inter-pass annealing. It was suggested that grain growth may or may not occur depending on the value of the dimensionless parameter Z_H given by [32]:

$$Z_H = 3f\overline{R}/2r \quad (3)$$

where $\overline{R}$ is the mean radius of grain assembly; f is the volume fraction of the second phase particles; and r is the mean radius of the spherical particles. The substitution of the structural parameters for the 1561HA1 and 1561HA2 alloys into Eq. (3) leads to $Z_H > 2$ for the 1561HA1 alloy and $0.3 < Z_H < 0.5$ for the 1561HA2 alloy. In accordance with Ref. [32], no grain growth can occur under static annealing when $Z_H > 1$, as in the case of the 1561HA1 alloy, irrespective of the size and shape of the separate grains [32], whereas Z_H lying in the range from 0.2 to 1 confirms the discontinuous growth of separate grains in the 1561HA2 alloy during the inter-pass annealing [32].

The relations $F_p > F_d$ and $Z_H > 2$ confirm that at low and high strains, there is no static grain growth in the 1561HA1 alloy, and the main factor of the UFG structure formation is a hot deformation. At $\varepsilon \leqslant 4$, the Al_6Mn dispersoids provide the stabilization of LABs. The dense array of LABs required for the occurrence of CDRX [8,10,11,25,26] is evolved at a strain of ~4 (Fig. 9a). A large number of mobile dislocations move across the subgrain interiors and are trapped by deformation-induced LABs, resulting in an increase in their misorientation followed by their transformation to HABs [10,11]. At $\varepsilon \geqslant 4$, a dispersion of Al_6Mn particles impedes the migration of HABs under both static and dynamic conditions. It is obvious that at $\varepsilon \geqslant 4$, the recrystallized grains persistently replace subgrains through the continuous transformation of LABs into HABs. Upon processing to a cumulative strain of $\varepsilon \approx 12$, the average misorientation in the 1561HA1 alloy continuously increases to ~28.5° (Fig. 8c), which is close to that of ~30° in the SPDed strain-induced grained materials with a face-centered-cubic (fcc) lattice [33]. The fraction of HABs, of ~0.66, approaches a typical value of 0.7 for recrystallized grained structures [8,34]. This structure is a granular one and is not susceptible to discontinuous grain growth [8,35–37] under static annealing.

On the other hand, the relations $F_p > F_d$ and $0.3 < Z_H < 0.5$ suggest that the deformation microstructure cannot undergo continuous grain growth, but discontinuous grain growth is still possible on annealing in the 1561HA2 alloy. The pinning force of $\sim 1.9 \times 10^5$ N m^{-2} exerted by the coarse Al_6Mn particles precipitated in the 1561HA2 alloy is not sufficient to impede the mobility of the separate grain boundaries under inter-pass annealing and to prevent discontinuous grain coarsening. An extensive collision of migrating LABs of opposite signs leads to their complete disappearance, which ceases the formation of a stable array of LABs [38,39]. As a result, the density of the deformation-induced LABs (Fig. 9) and their average misorientation in the 1561HA2 alloy are

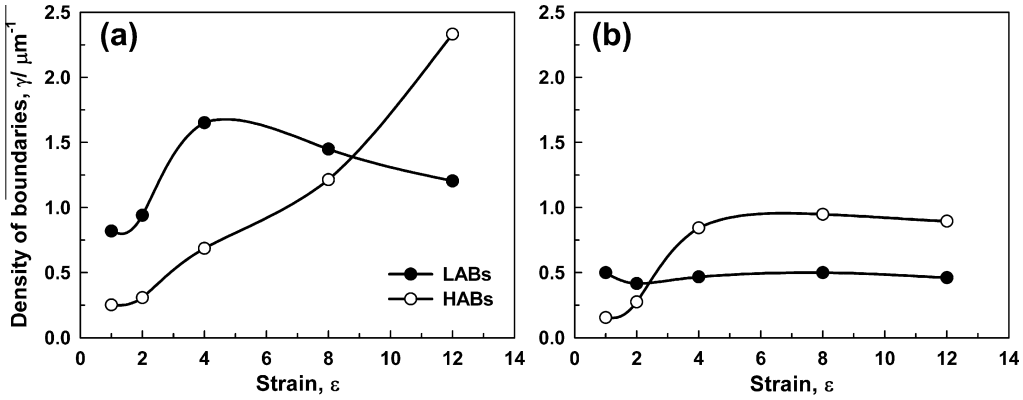

Fig. 9. Effect of strain on density of deformation-induced boundaries in the 1561HA1 (a) and 1561HA2 (b) alloys.

significantly lower than those in the 1561HA1 alloy. CDRX could not develop if an extensive collision of LABs took place at the initial stage of deformation [39]. At the same time, the recrystallized grains can easily grow statically into an array of dislocation boundaries with low misorientation. Furthermore, $Z_H < 0.5$ calculated for the 1561HA2 alloy indicates that the critical size of the recrystallized grains that are susceptible to discontinuous growth is relatively low [32], and, therefore, that numerous grains can grow discontinuously, which can be clearly seen in Figs. 5b–d and 7b–d. The coarse grains observed in the 1561HA2 alloy after ECAP are a result of the hot deformation and static recrystallization during the inter-pass annealing. The last process occurs because of the deficiency of the Zener drag force associated with a lack of nanoscale dispersoids [30,31].

It is worth noting that the size of the recrystallized grains achieved in the 1561HA1 alloy subjected to ECAP is less than the size of the fine recrystallized grains in Al–6% Mg–0.35% Sc alloy after ECAP at the same temperature [25], by a factor of ~2. This difference could not be attributed to the difference in Zener drag pressure alone. It is known [5] that if an alloying element provides solid solution strengthening and increases work hardening by reducing the rate of recovery, that element also reduces the grain size achieved in an aluminum alloy subjected to SPD. It is known that the presence of Zr within the aluminum solid solution strongly decreases the diffusivity through the aluminum matrix [40], inhibiting dynamic recovery and reducing the rate of dynamic boundary migration. As a result, the size of the dynamically recrystallized grains decreases. Thus, high Zener drag pressure exerted by the dispersion of the nanoscale particles of the Al_6Mn phase and the saturation of the solid solution by Zr, which decreases the diffusivity, allows the achievement of finer grain size in the 1561Al alloy than in the Al–6% Mg–0.35% Sc alloy [25].

5. Conclusions

The effect of the second phase particles on grain refinement in the 1561 aluminum alloy subjected to ECAP to a strain of ~12 at 300 °C was studied in the present work. The main results are summarized as follows:

1. Intermediate temperature HA at 360 °C leads to the precipitation of equiaxed nanoscale Al_6Mn dispersoids with an average size of ~25 nm. These particles have a high coarsening resistance at a temperature of ~300 °C. On the other hand, coarse plate-like Al_6Mn particles evolve in the 1561Al subjected to high-temperature HA at 440 and 500 °C.
2. At 300 °C, the nanoscale Al_6Mn dispersoids are as effective as the Al_3Sc dispersoids. The presence of the Al_6Mn dispersoids promotes dislocation generation and provides stabilization of the new grain boundaries during deformation and annealing. The formation of new grains under ECAP of the 1561Al alloy with nanoscale Al_6Mn dispersoids occurs through continuous dynamic recrystallization. At the initial stage of the deformation ($\varepsilon \leqslant 4$), three-dimensional arrays of LABs evolve homogeneously within the interiors of the original grains and along the initial grain boundaries. Further deformation leads to the gradual transformation of LABs into HABs at a high rate. A new fine-grained microstructure with an average grain size of ~0.55 μm develops at a strain of ~12 in the 1561Al.
3. A coarse-grained structure develops during ECAP in the 1561Al alloy subjected to high-temperature HA. The grain coarsening is caused by the fact that while the Zener drag force originating from coarse Al_6Mn particles is sufficient to suppress continuous grain growth during annealing between the ECAP passes, separate grains can still grow discontinuously due to deficiency of the Zener drag pressure.

Acknowledgements

This study was supported by the Department of Education and Science, Russian Federation, under Grant No. P977. The authors are grateful to the staff of the Joint Research Center, Belgorod State University, for their assistance with instrumental analysis.

References

[1] Davis JR. Aluminum and aluminum alloys. Materials Park, OH: ASM International; 1993.
[2] Valiev RZ, Langdon TG. Prog Mater Sci 2006;51:881.
[3] Hayes JS, Keyte R, Prangnell PB. Mater Sci Technol 2000;16:1259.
[4] Valiev RZ, Enikeev NA, Murashkin MYu, Kazykhanov VU, Sauvage X. Scr Mater 2010;63:949.
[5] Huang Y, Robson JD, Prangnell PB. Acta Mater 2010;58:1643.
[6] Jazaeri H, Humphreys FJ. Acta Mater 2004;52:3239.
[7] Apps PJ, Berta M, Prangnell PB. Acta Mater 2005;53:499.
[8] Humphreys FJ, Hatherly M. Recrystallization and related annealing phenomena. Oxford: Elsevier; 2005.
[9] Royset J, Ryum N. Int Mater Rev 2005;50:19.
[10] Nieh TG, Hsiung LM, Wadsworth J, Kaibyshev R. Acta Mater 1998;46:2789.
[11] Kaibyshev R, Avtokratova E, Apollonov A, Davies R. Scr Mater 2006;54:2119.
[12] Berta M, Apps PJ, Prangnell PB. Mater Sci Eng A 2005;410–411:381.
[13] Ning JL, Jiang DM. Mater Sci Eng A 2007;452–453:552.
[14] Barlow CY, Hansen N, Liu YL. Acta Mater 2002;50:171.
[15] Riddle YW, Sanders TH. Met Mater Trans A 2004;35:341.
[16] Mondolfo LF. Aluminum alloys: structure and properties. London: Butterworths; 1976.
[17] Hu R, Ogura T, Tezuka H, Sato T, Liu Q. J Mater Sci Technol 2010;26:237.
[18] Kaibyshev R, Musin F, Lesuer DR, Nieh TG. Mater Sci Eng A 2003;342:169.
[19] Nikulin I, Kipelova A, Malopheyev S, Kaibyshev R. Mater Trans 2011;52:882.
[20] Nakashima K, Horita Z, Nemoto M, Langdon TG. Acta Mater 1998;46:1589.
[21] Russ JC, Dehoff RT. Practical stereology. 2nd ed. New York: Kluwer Academic/Plenum; 2000.
[22] Hirsch PB, Howie A, Nicholson RB, Pashley DW, Whelan MJ. Electron microscopy of thin crystals. 2nd ed. New York: Krieger; 1977.
[23] Tomas G, Goringe MJ. Transmission electron microscopy of metals. New York: Wiley; 1979.
[24] Jia Z, Hu G, Forbord B, Solberg JK. Mater Sci Eng A 2007;444:284.
[25] Sitdikov O, Sakai T, Avtokratova E, Kaibyshev R, Tsuzaki K, Watanabe Y. Acta Mater 2008;56:821.
[26] Sitdikov O, Sakai T, Avtokratova E, Kaibyshev R, Kimura Y, Tsuzaki K. Mater Sci Eng A 2007;444:18.
[27] Kaibyshev R, Shipilova K, Musin F, Motohashi Y. Mater Sci Eng A 2005;396:341.
[28] Military handbook – MIL-HDBK-5H: Metallic materials and elements for aerospace vehicle structures. US Department of Defense; 2003.
[29] Murr EL. Interfacial phenomena in metals and alloys. Reading, MA: Addison-Wesley; 1975.
[30] Rios PR. Acta Mater 1997;45:1785.
[31] Rios PR. Scr Mater 1998;39:1725.
[32] Humphreys FJ. Acta Mater 1997;45:5031.
[33] Belyakov A, Sakai T, Miura H, Tsuzaki K. Phil Mag A 2001;81:2629.
[34] Humphreys FJ, Prangnell PB, Bowen JR, Gholinia A, Harris C. Phil Trans R Soc Lond A 1999;357:1663.
[35] Ferry M, Burhan N. Scr Mater 2007;56:525.
[36] Ferry M, Hamilton NE, Humphreys FJ. Acta Mater 2005;53:1097.
[37] Jazaeri H, Humphreys FJ. Acta Mater 2004;52:3251.
[38] Sitdikov O, Kaibyshev R. Mater Sci Eng A 2002;328:147.
[39] Biberger M, Blum W. Phil Mag A 1992;65:757.
[40] Doherty RD, Hughes DA, Humphreys FJ, Jonas JJ, Jensen DJ, Kassner ME, et al. Mater Sci Eng A 1997;238:219.